Journal of South American Earth Sciences
August 2023, Volume 128, Pages 104398 (11p)
https://doi.org/10.1016/j.jsames.2023.104398
https://archimer.ifremer.fr/doc/00836/94834/

Deep crustal structures with reverse time migration applied to offshore wide-angle seismic data: Equatorial and North-West Brazilian margins

Gonçalves Susana [1, 2, 3, *], Schnürle Philippe [1], Rabineau Marina [5], Afilhado A. [3, 4], Aslanian Daniel [1], Moulin Maryline [1], Evain Mikael [1], Loureiro A. [3], Dias N. [3, 4]

[1] Geo-Ocean, Univ Brest, CNRS, Ifremer, UMR6538, F-29280, Plouzane, France
[2] FCT – Fundação para a Ciência e Tecnologia, Av. D. Carlos I, No 126, 1249-074, Lisbon, Portugal
[3] IDL – Instituto Dom Luiz, Campo Grande, Edifício C1, Piso C1, 1749-016, Lisbon, Portugal
[4] ISEL – Instituto Superior de Engenharia de Lisboa, Rua Conselheiro Emídio Navarro, 1, 1959-007, Lisbon, Portugal
[5] Geo-Ocean, Univ Brest, CNRS, Ifremer, UMR6538, F-29280, Plouzane, France

* Corresponding author : Susana Gonçalves, email address : Susana.Goncalves@univ-brest.fr

Abstract :

We image the Moho discontinuity and deep crustal layers by applying the Reverse Time Migration (RTM) method to wide-angle seismic (WAS) data that were acquired along two different profiles in NW and SE offshore Brazil, where the spacing between OBS is 12.5 km and 150 m between shots. The application of this method is quite uncommon to ocean bottom seismometers (OBS) data due to the OBS wide spacing deployment and low folds.

We analyze the effectiveness of the RTM method when applied to the reflectivity of the WAS data. We imaged the structures by cross-correlating the forward and backward wavefields given by the acoustic seismic equation. This allowed us to use each interface crossed by a ray as both a source and a receiver. The velocity models used to perform RTM were previously obtained by applying a procedure of two-dimensional forward ray-tracing followed by a damped least-squares travel time inversion. The results obtained have an unexpected large contribution from the wavefield traveling as refractions within the Earth and, because of that, we can talk about recovering refractors from the RTM results. We obtained strong and continuous refractors for depths of 7–15 km that correspond to the basement and the Moho discontinuity. As we move landwards, the refractors that correspond to the Moho discontinuity disappear due to the deepening of the surface. Finally, we investigate how the slight change on the velocity model influences the result of the RTM method. The obtained results are promising for a wide range of applications at a crustal scale seismic exploration, with wide-angle seismic data.

Highlights

► Reverse time migration method with offshore Wide-Angle seismic. ► Imaging of deep structures as Moho discontinuity and basement of the basin. with reverse time migration method. ► Essential contribution of the refracted wave-field that allow to image the deep structures. ► Effectiveness of the reverse time migration method for wide angle data. ► Essential contribution in the absence of high resolution seismic data, since it is possible to image the deep structures without loosing the imaging of the shallow ones.

Keywords : Wide-Angle Seismic data, Reverse Time migration, Offshore Brazil, Refraction imaging, Deep crustal structures

1. Introduction

The Reverse Time Migration method (RTM) was first developed and applied around the 1980's decade. The purpose of the method is to image the sub-surface by having the correlation between the forward and backward wavefields that propagate according to the two-way acoustic wave equation and the boundary condition (Baysal et al., 1984, 1983; McMechan, 1983; Whitmore, 1983).

RTM has been largely applied to reflection datasets of different sources and geometry acquisitions where the instruments have short distances between them (Chang and McMechan, 1987; Liu et al., 2011). The application of the method to wide-angle seismic (WAS) data is uncommon due to low folds in Ocean Bottom Seismometers (OBS) deployment with wide spacing (Górszczyk et al., 2017; Kamei et al., 2012; Nakanishi et al., 2008; Shiraishi et al., 2022).

Imaging shallow subsurface structures is usually done in high-resolution reflection profiles with multichannel seismic streamer data (MCS) surveys. However, this kind of surveys frequently fail to image the deep crustal structures due to the limited length of the streamer. Also, these surveys are not always available due to restrictions of using streamer cables, limitations related to mammals or protected areas on the survey locations or even weather conditions. Being able to image the deep crustal layers through RTM method from WAS data can be a valuable addition to seismic data processing and imaging.

The velocity structures required to perform RTM can be estimated from several processes. In this study, we use RayINVR from Zelt and Smith (1992) which is an iterative procedure of two-dimensional forward ray-tracing followed by a damped least-squares travel time inversion.

The two wide-angle seismic profiles presented in this study are part of two different seismic experiments, acquired in collaboration between the Department of Marine Geosciences (IFREMER: Institut Français de Recherche pour l'Exploitation de la MER, France), the Laboratory of "Oceanic Geosciences" (IUEM: Institut Universitaire et Européen de la Mer, France), the Instituto Dom Luiz – Faculdade de Ciências de Lisboa (IDL-FCUL, Portugal), the Universidade de Brasília (UnB, Brazil), and PETROBRAS (Brazil): (i) MAGIC – Margins of brAzil, Ghana and Ivory Coast, described in (Aslanian et al., 2015); (ii) SALSA – Sergipe Alagoas Seismic Acquisition, described in (Aslanian et al., 2016).

During the MAGIC survey, five combined wide-angle, and reflection seismic profiles were acquired in the Pará-Maranhão-Barreirinhas-Ceará basins northern Brazil (figure 1). Their location is in the southward second 600-800-km-wide segment of the Equatorial Atlantic Ocean, between the São Paulo Fracture Zone to the north, and the Chain Fracture Zone to the south. The system can be described as a pull-apart passive margin, with two strike slip borders.

A pool of OBS belonging to IFREMER's Marine Geosciences Department (Auffret et al., 2004) was used for the offshore wide-angle acquisition and 3 profiles were extended onshore by using portable seismic stations from the Brazilian Geophysics instrument pool (Observatório Nacional, Rio de Janeiro). The seismic source consisted of a 7589 in^3 array of 18 airguns, towed 25 m below the sea level and fired every 60 s. Shots were also recorded by a 4.5 km long, 360-channel solid streamer towed at 12-15 m depth, 275 m behind the ship (Aslanian et al., 2021).

Forward modeling of these wide-angle data sets (Aslanian et al, 2021; Moulin et al, 2021; Schnürle et al., this issue) reveals an E-W lateral evolution of the oceanic crust spreading initiation with: (1) an unthinned continental crust below the São Luís Craton, where the crust is 33 km thick, (2) a 60 km wide necking domain below the Ilha de Santana Platform; (3) offshore, east of the continental slope, a 10 km-thick deep sedimentary basin resting on a 5 km thick crust interpret as exhumed lower continental origin on the top of an Anomalous Velocity Layer (AVL) probably made of intrusions of mantle-derived melts into the lower continental crust, or a mixture of them; (4) eastwards, the limit of the previous domain is marked by NW-SE aligned volcanoes and the disappearance of the AVL. The sedimentary succession becomes thinner (6 km) overlaying a proto-oceanic crust characterized by seismic velocities higher than "normal" oceanic crust in its upper part, but in continuity with the velocity described in the previous domain; (5) followed by a more characteristic but thin oceanic crust.

In a SE-NW alignment and within the location of the MC5 profile presented in this study as well as in Schnürle et al. (this issue), 6 main sectors can be distinguished: (1) Medio Coreaù and Ceará Central trust belt; (2) the Basin I composing the continental slope, the Parnaíba Platform and associated Piauí-Camocin and Ceará Basins; (3) Basin II; (4) intermediate Basin III; (5) the volcanic line to the SW of the southern São Paulo double Fracture Zone; (6) deep sea Basin in the São Paulo double Fracture Zone. The main goal of the MAGIC survey was to establish the segmentation of the Pará-Maranhão basin and to determine the crustal nature of its domains

The second experiment, SALSA, is composed by 12 profiles – 9 perpendicular to the coast with NW-SE orientation and 3 parallel to the coast with SW-NE orientation – acquired in the Jequitinhonha, Camamú-Almada, Jacuípe, and Sergipe-Alagoas basins, northeast Brazil. This experiment aimed to constrain the crustal structure, the segmentation, and the geodynamical setting of the different segments and of the Camamu triple junction, where the aborted Reconcavo-Tucano-Jatoba rift system connects with the Jequitinhonha-Camamu-Almada and Jacuípe-Sergipe-Alagoas rifts (Loureiro et al., 2018; Pinheiro et al., 2018; Loureiro et al., this issue; Evian et al., this issue; Aslanian et al., this issue). In this experiment, 222 OBS instruments were deployed offshore and 124 LSS (Land Seismic Stations from ON) to extend onshore 5 of the profiles – SL02, SL04, SL09 and SL12.

The SL04 profile (figure 1) is located in the far Northeast portion of the experiment, within the Sergipe-Alagoas basin. The area within the profile is composed by 3 main domains (NW to SE): (1) Onshore, continental slope and offshore part of the Alagoas basin with a 30 km thick crust of continental origin, thinning seawards up to 15 km; (2)In the double Ascension Fracture Zone, the continental crust further thins to 10 km and is underlain by a lens-shaped Anomalous Velocity Layer (AVL) up to 5 km thick. A volcanic edifice that belongs to the Pernambuco seamounts fills the fracture zone; (3) deep sea basin composed by a 6-7 km thick oceanic crust (Aslanian et al., 2016; Neves et al., 2016; Pinheiro et al., 2018; Loureiro et al., 2018)

In order to investigate the potential of RTM, we selected one NW-SE profile from each survey on both sides of the Pernambuco-Borborema area and in prolongation of each other (figure 1). Both of these profiles have coincident MCS streamer data and for SL04, there is an ION-GXT line previously acquired. Then, we are able to compare the results of the RTM migration with the PSDM migration done for that MCS streamer data. Thus we can validate the usefulness of the RTM method for refractions recorded with wide-spaced OBS to image deep crustal layers, such as, the Moho discontinuity.

2. Data

The wide-angle seismic data used in this study consists of two different profiles from two wide-angle seismic acquisition projects on the North-West and South-East offshore, Brazil. One of the profiles – MC5 – is located in the Equatorial margin and the other – SL04 – is located in the North-West Brazilian margin (figure 1).

The offshore part of the MC5 profile is composed by 44 OBS stations and has a length of 528 km. The chosen SALSA project profile is composed by 14 OBS stations and has a length of 158 km. The spacing between each OBS station is 12.5 km and the airguns were fired each 60s or 150m, approximately. MCS streamer data acquisition were simultaneously conducted.

The shooting on MC5 profile started at MC5OBS44 and ended to MC5OBS05. Due to shallow water on the shelf, it was not possible to continue the shooting up to the position of MC5OBS01. Also, all the OBS stations were retrieved, but MC5OBS43 did not register any data. For profile SL04, all the OBS stations were retrieved and the shooting was done from SL04OBS14 to SL04OBS01.

All OBS stations were composed by three-component geophones and a hydrophone sensor. Moho refractions were clearly observed in most of the vertical component of the geophone records.

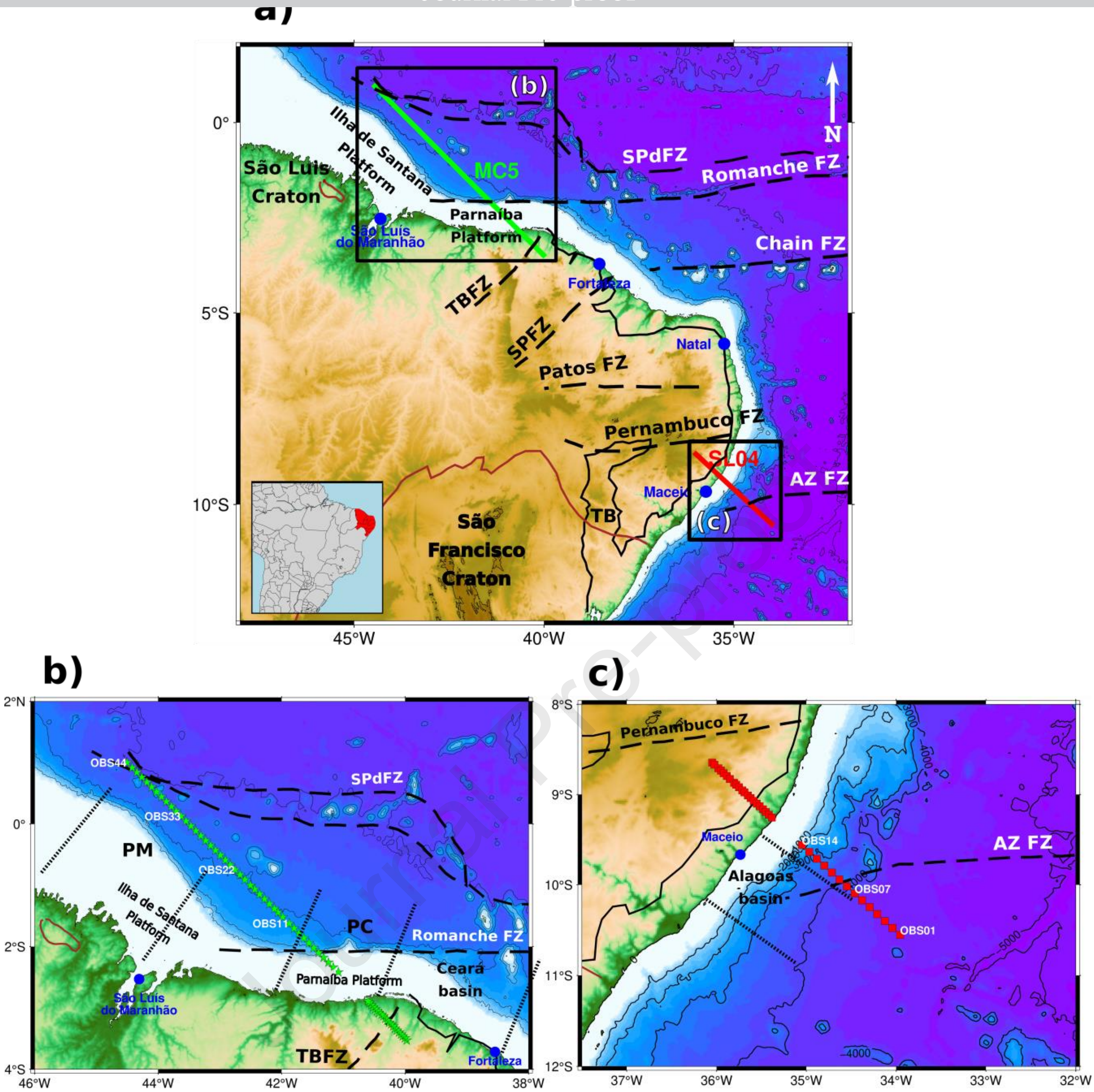

figure 1 - Location of the OBS stations for MC5 and SL04 profiles within Brazil. a) MC5 – green – is located to the North-West and SL04 – red – to the South-East of Borborema massif (SPdFZ - São Paulo double Fracture Zone; FZ - Fracture Zone; AZ FZ - Ascension Fracture Zone; TBFZ - TransBrasiliano Fracture Zone; SPFZ - Senador Pompeu Fracture Zone; TB - Tucano Basin; full black line – basin edges); b) Zoom on the OBS and LSS location for MC5 profile; (PM – Pará-Maranhão basin; PC – Piauí-Camocin basin) c) Zoom of the OBS and LSS location for SL04 profile

3. Method

The term that contemplates the time of propagation in the acoustic seismic equation, does not have a sense of positive or negative values. This means that the path taken by a particular ray can be traced back to the source by simply reverse the time to zero.

First we compute the forward propagating wavefield for each defined time step. Then, we restore the energy back to the respective sources by back-propagating the wavefield imposing the recorded signal as boundary condition for the same time steps. By correlating the forward and backward propagating wavefield for each saved time step, we image the horizons at their true vertical and horizontal positions.

In the case of pre-stack experiments, the shot profile reverse-time migration consists of a non-reflective two-way wave equation modeled with a finite difference (FD) method of the scalar acoustic wave equation. The method implemented is described in steps (Baysal et al., 1984; Nolet, 1986; Shiraishi et al., 2022). By adopting the source-receiver reciprocity on the relation between airgun shots and OBS's for each spacial coordinate in the model (x in equations (1), (2) and (3)), the down going wavefields – $F_i(x,t)$, equation (1) – are extrapolated forward in time from OBS locations (X_{OBSi} (i=1,2,…,M), equation (1)).The up going wavefields – $B_i(t,x)$, equation(2) – are extrapolated backwards in time from airgun shot locations (X_{shotj}, equation (2)) (e.g. (Schnürle et al., 2006; Shiraishi et al., 2022)):

1. We forward propagate a shot wavefield – $F_i(t,x)$ - in time (t: 0 → T) to out past all horizons (backward sorted), based on the scalar wave equation with a migration velocity – C(x) – and a source function – s(t) – from the ith OBS location – x_{OBSi} (i=1,2,…,M). The d(x-x_{OBSi}) is the Dirac delta function:

$$\left\{\frac{1}{C^2(x)}\frac{\partial^2}{\partial t^2} - \nabla^2\right\} F_i(t,x) = s(t)\delta\left(x - x_{OBS_i}\right) \qquad (1)$$

2. Back propagate the recorded wave field – $B_i(t,x)$ - at the same time interval (t: T → 0) by treating the seismic traces of the ith OBS record – $D_{i,j}(t,x_{shotj})$ – as a boundary condition at the sea surface:

$$\left\{\frac{1}{C^2(x)}\frac{\partial^2}{\partial t^2} - \nabla^2\right\} B_i(t,x) = \sum_{j=1}^{N} D_{i,j}\,(t,x\quad) \qquad (2)$$

3. Imaging – I(x) – by adding through all time steps the two wave field's product for each grid point. The imaging condition for the zero instance in the time domain can be represented by:

$$I(x) = \sum_{i=1}^{M} \int_0^T F_i\,(t,x) B_i(t,x) dt \qquad (3)$$

4. Finally we obtain the subsurface image along the entire profile by stacking the individual image sections from all OBS records.(Baysal et al., 1984; Nolet, 1986; Shiraishi et al., 2022)

4 . Data processing and Imaging

Figure 2 presents the raw geophone vertical component of three OBS from the MC5 profile, and highlights clear arrivals reflected from the Moho at each station.

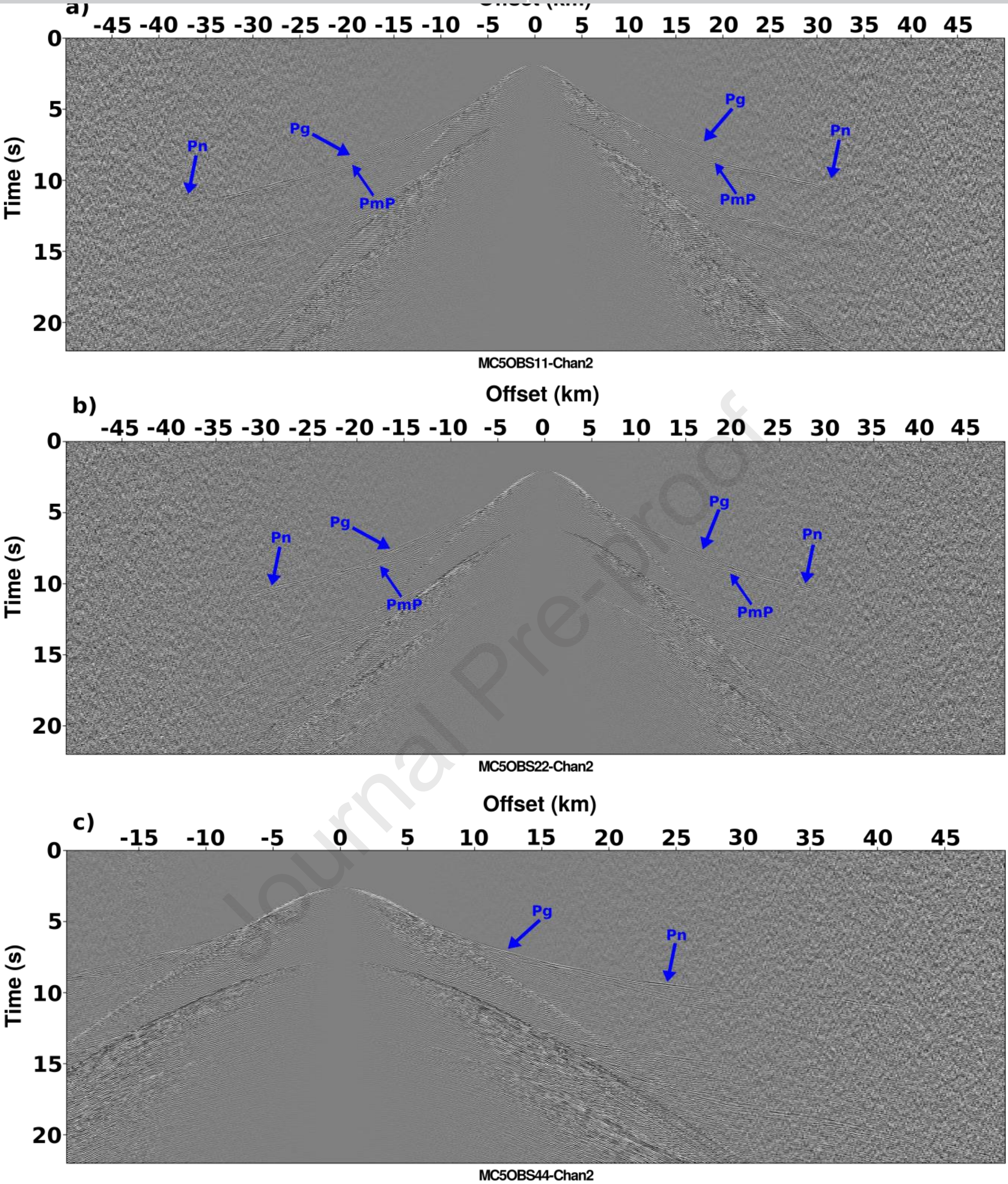

figure 2 – Examples of OBS acquired data for MC5 profile and examples of clear arrivals of the Moho for each station. a) MC5OBS11; b) MC5OBS22; c) MC5OBS44

The processing sequence consisted of 5 steps:

1) A wide butter-worth filter was applied in different intervals of lower frequencies – 0.5-4 Hz and high frequencies – 32-48 Hz, followed by spiking predictive deconvolution. To prevent noise from the water and other layer multiples, they were removed by applying mute. Finally, a narrower butter-worth filter of 1-4-12-18 Hz was applied(figure 3a).

2) To ensure sufficient resolution with limited dispersion and spacial aliasing, the optimal grid-spacing needs to be established. This grid-spacing was implemented in the 10^{th} order 2D finite difference acoustic modeling. Given the acquisition footprint, the horizontal grid spacing chosen is that of the shot spacing, i.e. dx=15 m. The recorded OBS data is sampled at 4 ms, and provided ample sampling for a vertical grid spacing dz=25 m. A grid with of 100 km (+/- 50 km offset) was selected in order to reach a depth of 25 km of imaging.

3) The layered RayINVR velocity models was converted into regular grids, the grids are cut in order to fit the section where the individual RTM OBS stations are placed and a damped least squares smoothing was applied. Applying the smoothing to the velocity model is essential in order for the migration technique to work and avoid artifacts generated by sharp variations of velocity for neighboring points.

4) The RTM migration was performed for each OBS station (figure 3b).

5)All individual RTM images were stacked in order to get the image for the entire set of stations within the entire profile (figure 3b). In order to enhance the migrated reflectors and refractors and avoid the artifacts generated by the large spacing between the OBS stations, prior to stacking, a dip filter was applied to each OBS obtained results , between -1.75 and 1.75and a final image was obtained (figure 3c).

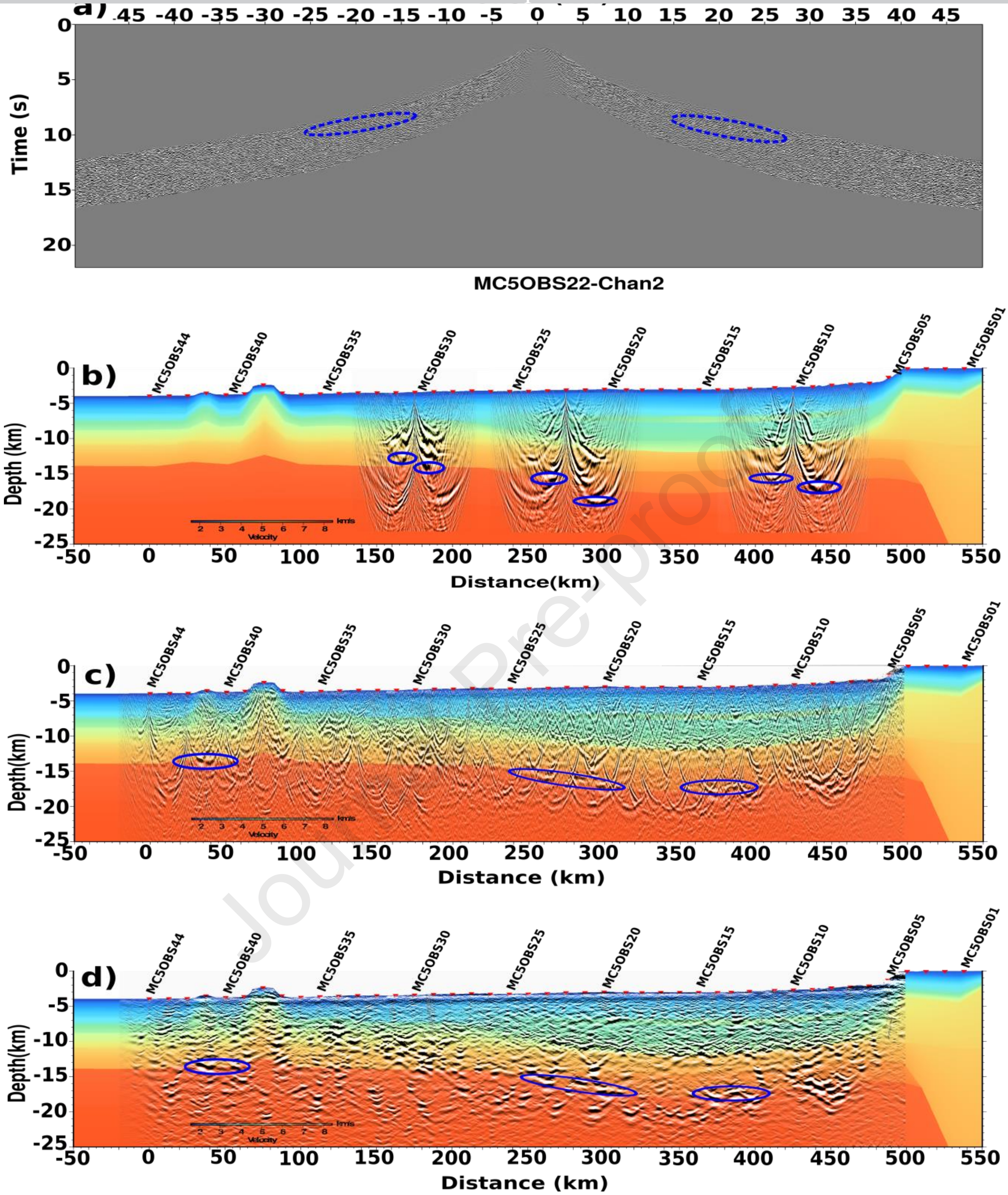

figure 3 – RTM imaging process for profile MC5. a) Processed data for MC5OBS22, channel 2; b) RTM image for MC5OBS10, MC5OBS22 and MC5OBS30 without dip filter applied overlaid with velocity model; c) Stacked result of the RTM section for MC5 profile with no dip filter applied; d) Stacked result of the RTM section for MC5 profile with dip filter applied. Vertical exaggeration 1:6

5. Results

The input data to perform the RTM for each OBS station contains reflected and refracted waves as we can observe from figure 2 (highlighted by the blue arrows).

The RTM result for station MC5OBS22 with the overlaid ray tracing - figure 4 - shows that we retrieve reflectors/refractors to offset distances of 60 km to each side of the OBS position. Also, the contribution of the refracted wave content is quite significant. For example, the Moho discontinuity is almost only illuminated by refracted waves – dark blue rays in figure 4.

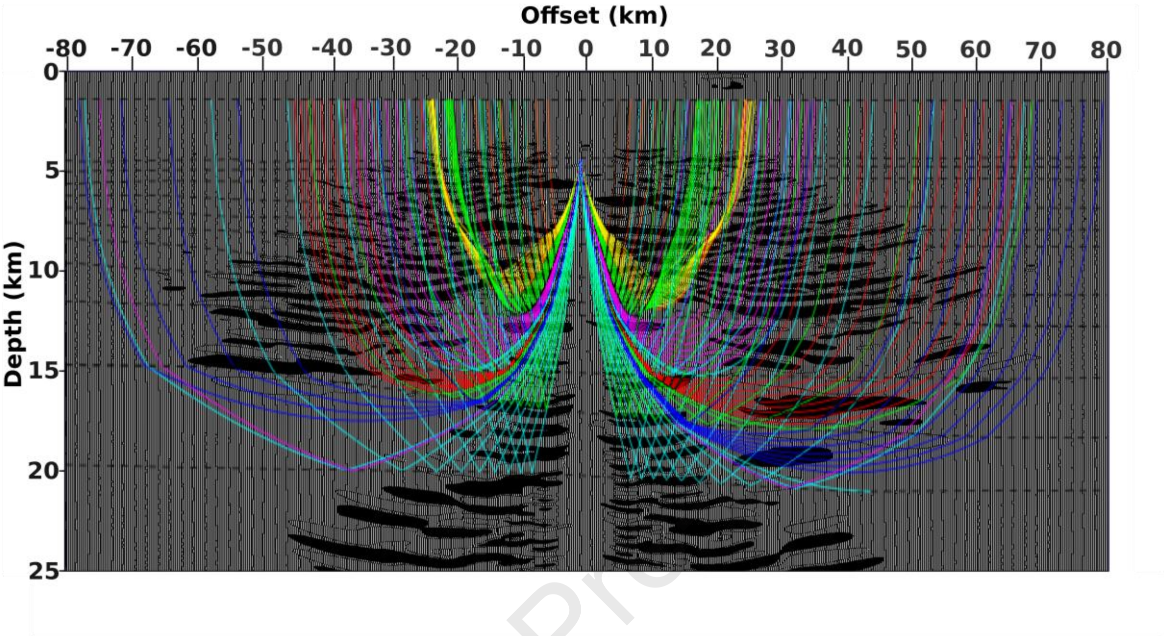

figure 4 – RTM results for MC5OBS22 overlaid with the ray tracing in our RayINVR velocity model

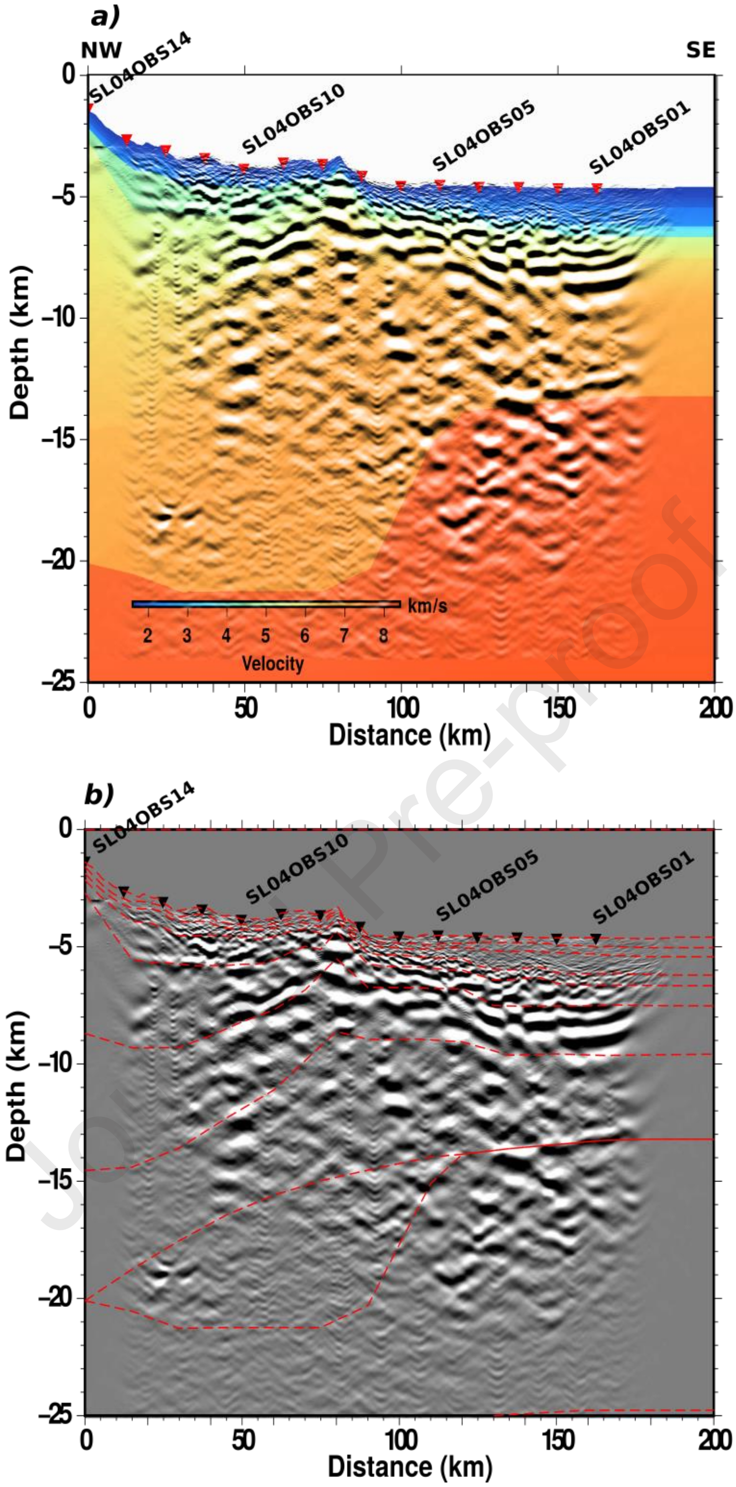

figure 5 – RTM results for profile SL04. a) RTM result overlaid over the velocity model; b) RTM result overlaid with layer interfaces – red dashed lines - of the velocity model. Vertical exaggeration 1:6

As shown in the stacked RTM results for both profiles – MC5 and SL04 in figures 3 and 5, respectively – several refractors are retrieved. The strongest and clearer are the ones that correspond to the basement of each basin and the Moho discontinuity. The retrieved refractors have a good match with the layer interfaces given by the velocity model.

For MC5 profile (figure 3), the basement of the basin refractor can be identified, between 10 and 12 km depth, for almost the entire length of the profile. It is less clear between 210 to 260 km distance (MC5OBS24 to MC5OBS28). The Moho discontinuity refractors can be identified between 14 to 17 km depth. In spite of their strength, they are not as continuous along the profile. The AVL refractors can also be identified at 14 km depth between 250 to 300 km distance and 400 to 475 km distance. At 5-6 km depth, within the basin – between 275 to 450 km distance - the higher velocity volcanic layer refractors are present. The refractors under the volcanic structures between 25 and 140 km are strong but the connection with the interfaces given by the velocity model is hard to do.

For SL04 profile (figure 5a), the base of the basin refractor at 5 km depth, is continuous and strong for the entire profile. Also, between 6 and 8 km depth, the refractor that corresponds to the base of the middle crust is also strong and continuous between 40 and 175 km distance. The Moho discontinuity refractor is at 14 km depth, visible between 130 and 175 km distance. From figure 5b, where the contours of the velocity model layer are presented (red dashed lines), the mentioned refractors match the velocity layers described. The refractors under the volcanic structure present in this profile are also strong. It is not possible to distinguish refractors that correspond to the layers that are within the basin and present in the velocity model.

6. Discussion

From the results presented in figure 4, the contribution of the refracted wavefield is essential for the imaging of several refractors, in particular the deeper ones. The basement, the AVL and the Moho discontinuity are imaged almost fully by refracted waves. Imaging the horizontal extent of the interfaces is also mostly supported by the refracted content. This large contribution becomes very important for the success of the RTM method and, although unexpected, highlights their importance for the quality of the seismic imaging. Since the refracted waves contribution are a large part of the energy of the wavefield traveling within the earth we can name the obtained interfaces as refractors.

From the stacked RTM results for each profile (figures 3d and 5 – MC5 and SL04, respectively), we obtained several refractors for different depths that match the layers given by the velocity models. The Moho discontinuity refractors – 18 km depth for MC5 profile – are the deeper ones that the method is able to retrieve, for the studied profiles. Not all the obtained refractors have a continuous behavior for the entire distance of the profiles but it is possible to interpolate between them.

For SL04 (figure 5), the basement, the upper crust, middle crust and the Moho discontinuity refractors are continuous and strong for the most offshore part. However, from 115 km model distance (SL04OBS05) and moving landwards, the refractors the correspond to the Moho discontinuity lose amplitude and eventually disappear. The Moho discontinuity seems to deepen abruptly with possible occurrence of an approximately 5 km thick additional AVL. The presence of refractor at the end of the profile – 25 km to 40 km model distance (SL04OBS12 to SL04OBS13) – just above AVL/Moho discontinuity depth, reinforce the structure present in the velocity model for a layered crust and the depth of the Moho discontinuity.

In MC5 (figure 3d), between 250 to 500 km distance, the presence of an AVL (Schnürle et al., this issue), that introduces a slower vertical velocity gradient when compared with the remaining offshore profile, seem to affect the resulting refractors that match the Moho discontinuity (Aslanian et al., 2021).

Both profiles have the presence of volcanic structures and they have an influence on the obtained results. In SL04 (figure 5a) the refractors under the volcano structure seem to be affected just until the upper crust depth (5 to 6 km depth, at 75 km distance). While the refractors within the volcanic structure seem to give continuity to the top of the upper crust, the refractors of the basement and other at shallower depths seem to be interrupted in the lateral of the volcano structure. For MC5 (figure 3d) the volcano structure is bigger and wider. All the obtained refractors located between 25 to 125 km seem to be affected by the structure and is hard to follow the refractors that correspond to the different layers. The volcanic structure seem to extend in depth up until the Moho discontinuity, at 14 km depth. Also, the strong oblique refractors present between 100 to 200 km distance and 8 to 14 km depth, suggest that the deeper layers may have played an important role upon the formation of those volcanic structures.

There is a significant difference in the strength and continuity of the obtained refractors between the two studied profiles. They have quite similar acquisition and processing parameters. The main difference between the profiles is their length and the velocity model used. The amplitude absorption and phase distortion linked with the specific composition of each layer, are the two main factors that affect the structure imaging and interface interpretation and, consequently, the RTM result (Wang et al., 2018; Zhang et al., 2013; Zhu et al., 2014). Comparing both profiles, the number and composition of the sedimentary layers, present on each basin, and an additional lithospheric crust layer on SL04 profile, are the main differences. For example, on the sedimentary basin of MC5, the presence of a thin volcanic ashes layer (Aslanian et al., 2021; Schnürle et al., this issue) – faster, denser, and very clear on the migration result – may act as an attenuation zone, dissipating seismic energy.

The pertinence of WAS RTM and its efficiency when compared to pre-stack depth migration (PSDM) of multi-channel seismic reflection data needs to be investigated. On figure 6, we present the comparison for SL04 between the PSDM GTX-2400 (an industrial survey conducted by ION with a ~12 km long streamer at the same location), the MCS streamer PSDM, and the RTM results for the same profile. On top of each result, we overlaid the interpreted line-drawing of GTX-2400.

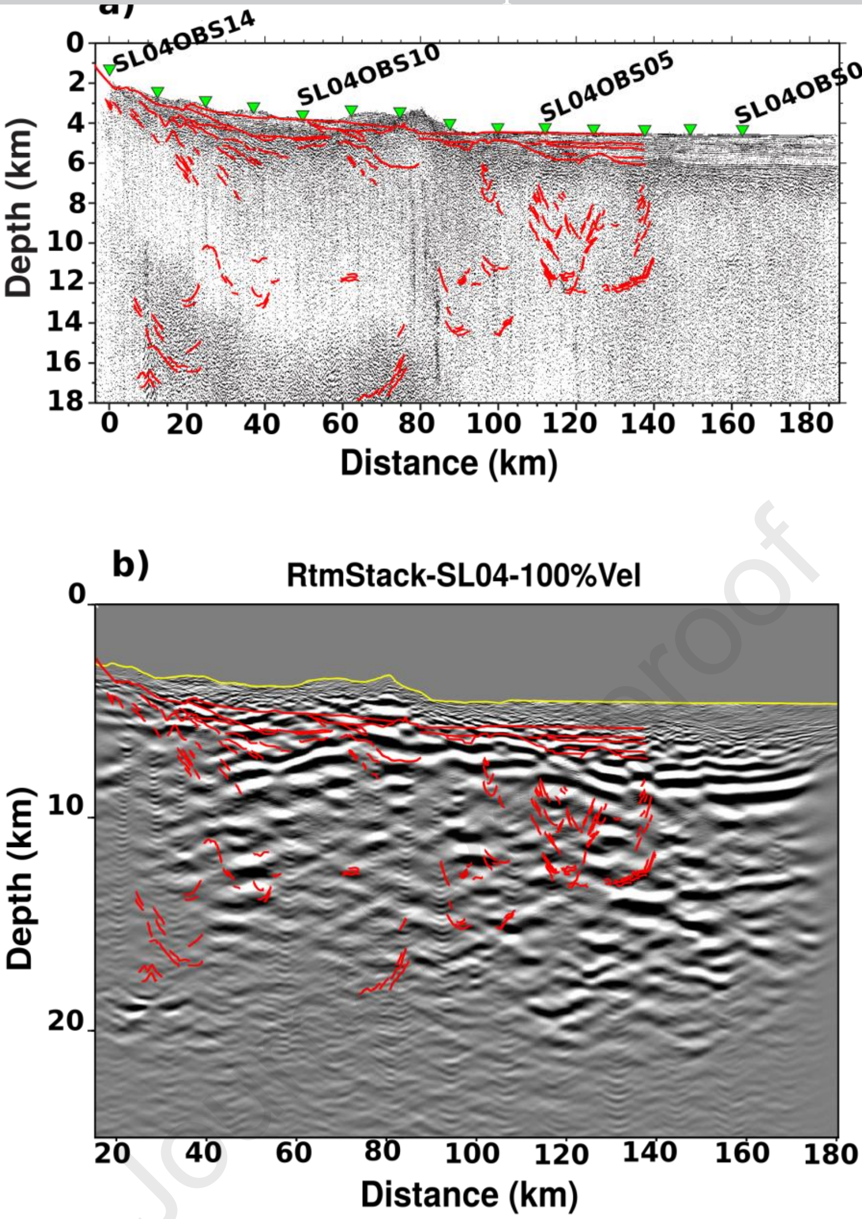

figure 6 – Comparison between PSDM and RTM migration method. a) PSDM results of the MCS streamer data for profile SL04 with overlaid ION-GXT 2400 interpreted line-drawing – red lines, which location overlaps the SL04 profile from SL04OBS14 to SL04OBS03; b) RTM results of the WAS data for profile SL04 with overlaid ION-GXT 2400 interpreted line-drawing – red lines. Vertical exaggeration 1:6

When we compare the PSDM results of MCS streamer data and the RTM results of the WAS data with the interpretation of the ION-GTX-2400 line, we can easily see that for shallow depths – up until the basement – we obtain quite similar results. However, for deeper layers, the PSDM results are insufficient to obtain crustal layers and the Moho discontinuity: refractors or reflectors are absent or mostly imperceptible for depths greater then 8-10 km. On the other hand, in the RTM results, we can identify refractors related with the crustal layers and the Moho discontinuity matching the discontinuous interpretation of the ION-GTX-2400 line. Furthermore, the obtained results reinforce the utility of the RTM method when applied to WAS data not only by showing that the results are trustworthy, but also that we can easily obtain an image of the subsurface with only WAS data, as previously done by (Shiraishi et al., 2022) .

The used velocity model to perform the RTM is one of the essential elements of the method. Therefore, an evaluation on how changes in the velocity model grid affect the obtained RTM results was performed for both profiles – figures 7 and 8. We preformed the RTM for overall slower velocity models - -4% (dark blue line in figure 7a to 7e) and -2% (cyan line in figure 7a to 7e) of the original (red line in figure 7a to 7e) – and faster velocity models - +2% (yellow line in figure 7a to 7e) and +4% (orange line in figure 7a to 7e). In figures 7a to 7e, we present the vertical velocity variation for five different model distances along MC5 profile. In figures 7f to 7j, the stacked RTM results are presented, for the each velocity model at five different model distances of MC5 profile. In figure 8 we present the RTM results for SL04, for each velocity model at two different model distances.

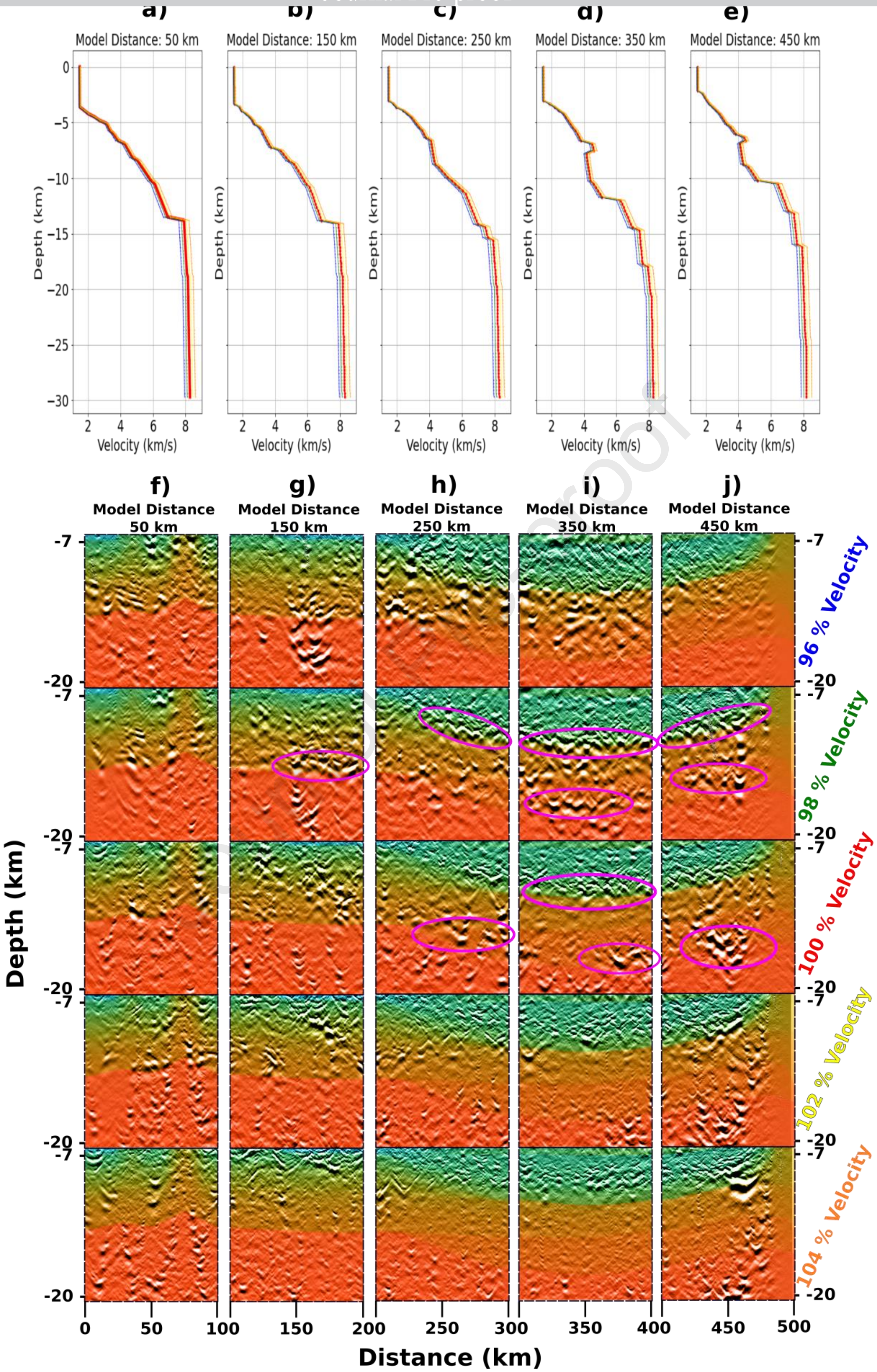

a)
b)
c)
d)
e)
Model Distance: 50 km
Model Distance: 150 km
Model Distance: 250 km
Model Distance: 350 km
Model Distance: 450 km
Depth (km)
Velocity (km/s)
f)
g)
h)
i)
j)
Model Distance 50 km
Model Distance 150 km
Model Distance 250 km
Model Distance 350 km
Model Distance 450 km
96 % Velocity
98 % Velocity
100 % Velocity
102 % Velocity
104 % Velocity
Depth (km)
Distance (km)

figure 7 - Effect of the variation of the velocity grids – -4%, -2%, +2% and +4% of the original – on the RTM results of MC5 profile. . Vertical variation of the velocity for different model distance: a) 50 km; b) 150 km; c) 250 km; d) 350 km; e) 450 km; RTM results overlaid by each velocity model for different model distance: f) 50 km ; g) 150 km ; h) 250 km ; i) 350 km ; j) 450 km. Vertical exaggeration 1:6

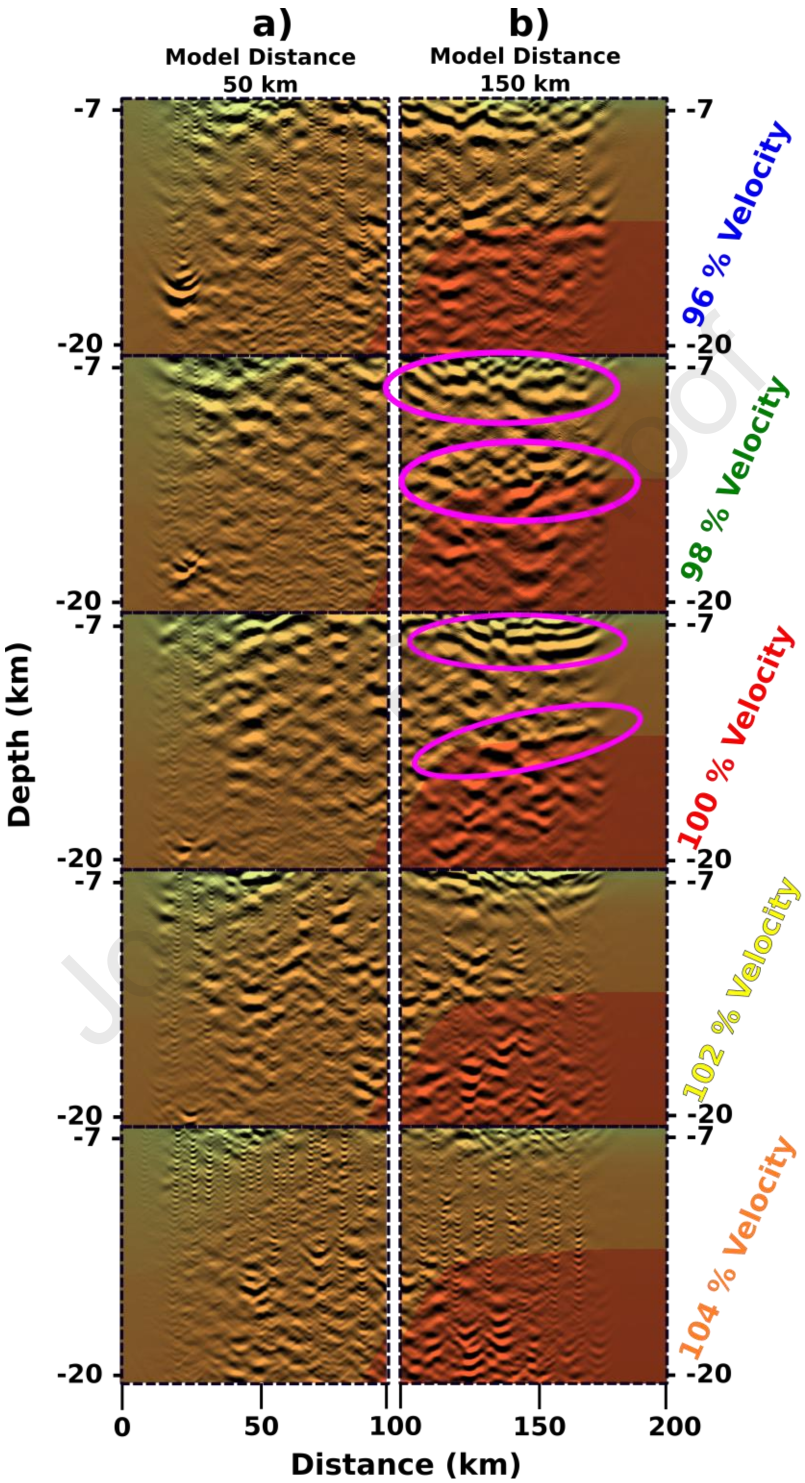

figure 8 - Effect of the variation of the velocity grids – -4%, -2%, +2% and +4% of the original – on the RTM results for SL04 profile. RTM results overlaid by each velocity model for different model distance: a) 50 km ; b) 150 km Vertical exaggeration 1:6

We can see that the velocity changing is uniform throughout the MC5 profile (figure 7a to 7e) and does not create any vertical variation that was not present on the original model (red line on figure 7a to 7e). Also, the quality of the RTM results is quite similar trough out the profile, being coherent with the previous point. On the other hand, the major feature that we observe is the different strengths of the refractors depending on the velocity model used. In the case of the MC5 profile (figure 7f to 7j), we observe that the basement and Moho refractors are quite good for the original velocity model but seem stronger for a velocity model that has 98% of the velocities of the original one. For the other velocity models – 96%, 102% and 104% - the same refractors are quite weak or even absent.

We performed the same analysis for SL04 (figure 8). The obtained results are similar to the ones obtained with MC5. However, for this profile, the refractors corresponding to the basement and Moho discontinuity are slightly stronger for the original velocity model but also quite good for the 96% and 98%.

There are a few reasons that can explain the different RTM results depending on the velocity model: (i) in spite of the ratio of velocity scaling is a few percent, the cumulative velocity difference from the seafloor to the target depth may have a strong effect on the focusing of the refractions (Shiraishi et al., 2022); (ii) the sensitivity to velocity structures could be high because of low folds of wide-angle data obtained with a spacing between OBS stations (Shiraishi et al., 2022); (iii) the uncertainty associated with the velocities of each layer, in particular the deeper ones; (iv) the geometry of the layers may contribute to the obtained results since, for example, for model distance of 250 km and 96% of the velocity model – MC5, figure 7h – and model distance 50 km and 96% of the velocity model – SL04, figure 7a – we obtain stronger refractors for the basement and Moho, respectively. For both cases, the layers have a stronger dip for those distances.

7. Conclusion

The main purpose of this study was to be able to image the deeper crustal layers by applying the RTM method to WAS data. This goal was clearly fulfilled since we were able to image the lithospheric crustal layers and the Moho discontinuity with success and also obtain the refractors that correspond to sedimentary layers at shallower depths. The refractors obtained match the layer based travel-time inversion models of the two studied areas (MC5: Schnürle et al., this issue; SL04: Aslanian et al., 2016).

The contribution of the energy traveling as refraction within the earth is relevant and is key on the obtained seismic depth images. The refracted waves are the main content that allow to image the base of the basin, the crustal layers and the Moho discontinuity in both profiles (figures 3d, 4 and 5). Without this refracted content within the wavefield, the characterization of the deeper layers geometry would not be as efficient or even impossible with the RTM method. This result is unexpected but very important.

The difference in amplitude and continuity of the refractors between the two profiles is quite clear (figures 3d and 4a). The number and composition of each layer present in the velocity models should explain the difference. Differences in amplitude absorption due to those characteristics and the depth of the target interfaces may explain the observed differences (Wang et al., 2018; Zhang et al., 2013; Zhu et al., 2014). However, further studies should be done to better understand it.

By comparing the PSDM results with the RTM (figure 6), we were able to confirm that we can better image the deeper crustal layers by using this method applied to the wide-angle data and also obtain the refractors that correspond to the shallower layers. We showed that the method is trustworthy and quite useful when the MCS streamer data are not available at the target depths, or can not be at all acquired.

By making variations of the overall velocity model between -4% and 4% (MC5 – figure 7; SL04 – figure 8), we have showed that the method is quite sensitive to velocity changes that could be related with the overall increase/decrease of velocity but may also be explained by the geometry of the target interfaces and, finally, with the uncertainties in the velocity of the deeper layers.

The general results have significance and are an important contribution for the seismic interpretation of the studied areas. The method allows to retrieve the main structures of the subsurface and reach depths that other migration methods are not capable. The method can be applied as a complement to other methods (PSDM or P-wave velocity modeling) and confirm or not the obtained results or it can be applied as a tool to retrieve the characteristics of deeper layers when only WAS data are available.

The MC5 profile RTM results (figure 3d), support the NW-SE segmentation in different basins, with different characteristics. In depth, the presence of a anomalous velocity layer just above the Moho discontinuity and the geometry of the basement and Moho discontinuity are also imaged by the RTM (Aslanian et al, 2021; Moulin et al, 2021; Schnürle et al., this issue). In SL04 (figure 4a), the imaging of the basement and the Moho discontinuity are also imaged and the geometry of the correspondent refractors enforce previous interpretations of having a continental crust with a rapid thinning seawards, the AVL under the thinned continental crust and a deep sea basin offshore with a thickness of approximately 6-7 km (Aslanian et al., 2016; Neves et al., 2016; Pinheiro et al., 2018; Loureiro et al., 2018).

These results were obtained from a data set where the OBS spacing, for the two profiles, is 12.5 km. Also, the velocity models used are quite complex in terms of geometry and velocity change. These characteristics contribute to potential amplitude absorption, phase distortion. The velocity uncertainties need to be taken into account. This gives to the RTM imaging method a great potential on diverse applications on wide-angle seismic data to study and explore at a crustal scale.

Acknowledgments

The authors would like to thank for the financial support from CAPES-COFECUB. This work was supported by ISblue project, Interdisciplinary graduate school for the blue planet (ANR-17-EURE-0015) and co-funded by a grant from the French government under the program "Investissements d'Avenir" embedded in France 2030.
We would like to thank to the supervisors who helped to develop the research presented in this manuscript and to the researcher that help improve the writing and the quality of this manuscript.

Funding

This PhD of S. Gonçalves was funded by the Portuguese Fundação para a Ciência e a Tecnologia (FCT) I.P./MCTES through national funds (PIDDAC) – SFRH/BD/145433/2019. This research was funded by Petrobras (Brazil) and Ifremer (France). The data set collected during the MAGIC and SALSA experiments are protected under a partnership with Petrobras. Any request has to be addressed to Daniel Aslanian (aslanian@ifremer.fr) and Adriano Viana (aviana@petrobras. com.br).

8. References

Aslanian, D., Gallais, F., Afilhado, A., Schnurle, P., Moulin, M., Evain, M., Dias, N., Soares, J., Fuck, R., da Cruz Pessoa Neto, O., Viana, A., 2021. Deep structure of the Pará-Maranhão/Barreirinhas passive margin in the equatorial Atlantic (NE Brazil). Journal of South American Earth Sciences 110, 103322. https://doi.org/10.1016/j.jsames.2021.103322

Aslanian, D., Moulin, M., Afilhado, A., Gallais, F., Schnurle, P., Dias, N., Benabdellouahed, M., Baltzer, A., Rabineau, M., 2015. Wide-Angle and Multi-Channel Seismic Experiment in the Maranhão–Barreirinhas-Ceará Basins (Brazil) (Field report).
Aslanian, D., Moulin, M., Evian, M., Afilhado, A., Schnürle, P., Gallais, F., Loureiro, A., Pinheiro, J.M., Klingelhoefer, F., Dias, N., Rabineau, M., Baltzer, A., Benabdellouahed, M., 2016. Wide-Angle and Multi-Channel Seismic Experiment in the Jequitinhonha-CamamúJacuípe-Alagoas-Sergipe Basins (NE Brazil) (Field report). Ifremer.
Auffret, Y., Pelleau, P., Klingelhoefer, F., Geli, L., Crozon, J., Lin, J.Y., Sibuet, J.-C., 2004. MicrOBS: A new generation of ocean bottom seismometer. First Break 22. https://doi.org/10.3997/1365-2397.2004012
Baysal, E., Kosloff, D.D., Sherwood, J.W.C., 1984. A two-way nonreflecting wave equation. GEOPHYSICS 49, 132–141. https://doi.org/10.1190/1.1441644
Baysal, E., Kosloff, D.D., Sherwood, J.W.C., 1983. Reverse time migration. GEOPHYSICS 48, 1514–1524. https://doi.org/10.1190/1.1441434
McMechan, G.A., 1983. Migration by extrapolation of time-dependent boundary values. Geophys. Prosp. 31, 413–420.
Moulin, M., Schnurle, P., Afilhado, A., Gallais, F., Dias, N., Evain, M., Soares, J., Fuck, R., da Cruz Pessoa Neto, O., Viana, A., Aslanian, D., 2021. Imaging Early Oceanic Crust spreading in the Equatorial Atlantic Ocean: Insights from the MAGIC wide-angle experiment. Journal of South American Earth Sciences 111, 103493. https://doi.org/10.1016/j.jsames.2021.103493
Neves, S.P., Rangel da Silva, J.M., Bruguier, O., 2016. The transition zone between the Pernambuco-Alagoas Domain and the Sergipano Belt (Borborema Province, NE Brazil): Geochronological constraints on the ages of deposition, tectonic setting and metamorphism of metasedimentary rocks. Journal of South American Earth Sciences 72, 266–278. https://doi.org/10.1016/j.jsames.2016.09.010
Pinheiro, J.M., Schnurle, P., Evain, M., Afilhado, A., Gallais, F., Klingelhoefer, F., Loureiro, A., Fuck, R., Soares, J., Cupertino, J.A., Viana, A., Rabineau, M., Baltzer, A., Benabdellouahed, M., Dias, N., Moulin, M., Aslanian, D., Morvan, L., Mazé, J.P., Pierre, D., Roudaut-Pitel, M., Rio, I., Alves, D., Barros Junior, P., Biari, Y., Corela, C., Crozon, J., Duarte, J.L., Ducatel, C., Falcão, C., Fernagu, P., Le Piver, D., Mokeddem, Z., Pelleau, P., Rigoti, C., Roest, W., Roudaut, M., 2018. Lithospheric structuration onshore-offshore of the Sergipe-Alagoas passive margin, NE Brazil, based on wide-angle seismic data. Journal of South American Earth Sciences 88, 649–672. https://doi.org/10.1016/j.jsames.2018.09.015
Whitmore, N.D., 1983. Iterative depth migration by backward time propagation, in: SEG Technical Program Expanded Abstracts 1983. Presented at the SEG Technical Program Expanded Abstracts 1983, Society of Exploration Geophysicists, pp. 382–385. https://doi.org/10.1190/1.1893867lanian, D., Gallais, F., Afilhado, A., Schnurle, P., Moulin, M., Evain, M., Dias, N., Soares, J., Fuck, R., da Cruz Pessoa Neto, O., Viana, A., 2021. Deep structure of the Pará-Maranhão/Barreirinhas passive margin in the equatorial Atlantic (NE Brazil). Journal of South American Earth Sciences 110, 103322. https://doi.org/10.1016/j.jsames.2021.103322
Aslanian, D., Moulin, M., Evain, M., 2016. Wide-Angle and Multi-Channel Seismic Experiment in the Jaquitinhonha-Camamú-Jacuípe-Alagoas-Sergipe Basins (NE Brazil).
Baysal, E., Kosloff, D.D., Sherwood, J.W.C., 1984. A two-way nonreflecting wave equation. GEOPHYSICS 49, 132–141. https://doi.org/10.1190/1.1441644
Baysal, E., Kosloff, D.D., Sherwood, J.W.C., 1983. Reverse time migration. GEOPHYSICS 48, 1514–1524. https://doi.org/10.1190/1.1441434
Chang, W., McMechan, G.A., 1987. Elastic reverse-time migration. GEOPHYSICS 52, 1365–1375. https://doi.org/10.1190/1.1442249

Gorszczyk, A., Operto, S., Malinowski, M., 2017. Toward a robust workflow for deep crustal imaging by FWI of OBS data: The eastern Nankai Trough revisited: FULL-WAVEFORM INVERSION OF OBS DATA. J. Geophys. Res. Solid Earth 122, 4601–4630. https://doi.org/10.1002/2016JB013891

Kamei, R., Pratt, R.G., Tsuji, T., 2012. Waveform tomography imaging of a megasplay fault system in the seismogenic Nankai subduction zone. Earth and Planetary Science Letters 317–318, 343–353. https://doi.org/10.1016/j.epsl.2011.10.042

Liu, Y., Chang, X., Jin, D., He, R., Sun, H., Zheng, Y., 2011. Reverse time migration of multiples for subsalt imaging. GEOPHYSICS 76, WB209–WB216. https://doi.org/10.1190/geo2010-0312.1

Loureiro, A., Schnürle, P., Klingelhöfer, F., Afilhado, A., Pinheiro, J., Evain, M., Gallais, F., Dias, N.A., Rabineau, M., Baltzer, A., Benabdellouahed, M., Soares, J., Fuck, R., Cupertino, J.A., Viana, A., Matias, L., Moulin, M., Aslanian, D., Morvan, L., Mazé, J.P., Pierre, D., Roudaut-Pitel, M., Rio, I., Alves, D., Barros Junior, P., Biari, Y., Corela, C., Crozon, J., Duarte, J.L., Ducatel, C., Falcão, C., Fernagu, P., Vinicius Aparecido Gomes de Lima, M., Le Piver, D., Mokeddem, Z., Pelleau, P., Rigoti, C., Roest, W., Roudaut, M., 2018. Imaging exhumed lower continental crust in the distal Jequitinhonha basin, Brazil. Journal of South American Earth Sciences 84, 351–372. https://doi.org/10.1016/j.jsames.2018.01.009

McMechan, G.A., 1983. Migration by extrapolation of time-dependent boundary values. Geophys. Prosp. 31, 413–420.

Moulin, M., Schnurle, P., Afilhado, A., Gallais, F., Dias, N., Evain, M., Soares, J., Fuck, R., da Cruz Pessoa Neto, O., Viana, A., Aslanian, D., 2021. Imaging Early Oceanic Crust spreading in the Equatorial Atlantic Ocean: Insights from the MAGIC wide-angle experiment. Journal of South American Earth Sciences 111, 103493. https://doi.org/10.1016/j.jsames.2021.103493

Nakanishi, A., Kodaira, S., Miura, S., Ito, A., Sato, T., Park, J.-O., Kido, Y., Kaneda, Y., 2008. Detailed structural image around splay-fault branching in the Nankai subduction seismogenic zone: Results from a high-density ocean bottom seismic survey. J. Geophys. Res. 113, B03105. https://doi.org/10.1029/2007JB004974

Nolet, G., 1986. Imaging the Earth's Interior, J. F. Claerbout, Blackwell Scientific Publications, Oxford, 1985 414pp., 42.00 and Fundamentals of Geophysical Data Processing, 2nd edn J. F. Claerbout, Blackwell Scientific Publications, Oxford, 1985 274 pp., 42.00. Geophysical Journal International 86, 217–219. https://doi.org/10.1111/j.1365-246X.1986.tb01086.x

Pinheiro, J.M., Schnurle, P., Evain, M., Afilhado, A., Gallais, F., Klingelhoefer, F., Loureiro, A., Fuck, R., Soares, J., Cupertino, J.A., Viana, A., Rabineau, M., Baltzer, A., Benabdellouahed, M., Dias, N., Moulin, M., Aslanian, D., Morvan, L., Mazé, J.P., Pierre, D., Roudaut-Pitel, M., Rio, I., Alves, D., Barros Junior, P., Biari, Y., Corela, C., Crozon, J., Duarte, J.L., Ducatel, C., Falcão, C., Fernagu, P., Le Piver, D., Mokeddem, Z., Pelleau, P., Rigoti, C., Roest, W., Roudaut, M., 2018. Lithospheric structuration onshore-offshore of the Sergipe-Alagoas passive margin, NE Brazil, based on wide-angle seismic data. Journal of South American Earth Sciences 88, 649–672. https://doi.org/10.1016/j.jsames.2018.09.015

Schnurle, P., Liu, C.-S., Lee, C.-S., 2006. Acoustic and Shear-Wave Velocities in Hydrate-Bearing Sediments Offshore Southwestern Taiwan: Tomography, Converted Waves Analysis and Reverse-Time Migration of OBS Records. Terr. Atmos. Ocean. Sci. 17, 757. https://doi.org/10.3319/TAO.2006.17.4.757(GH)

Shiraishi, K., No, T., Fujie, G., 2022. Seismic reflection imaging of deep crustal structures via reverse time migration using offshore wide-angle seismic data on the eastern margin of the Sea of Japan. Earth Planets Space 74, 28. https://doi.org/10.1186/s40623-022-01590-w

Wang, Y., Zhou, H., Chen, H., Chen, Y., 2018. Adaptive stabilization for *Q* -compensated reverse time migration. GEOPHYSICS 83, S15–S32. https://doi.org/10.1190/geo2017-0244.1

Whitmore, N.D., 1983. Iterative depth migration by backward time propagation, in: SEG Technical Program Expanded Abstracts 1983. Presented at the SEG Technical Program Expanded Abstracts 1983, Society of Exploration Geophysicists, pp. 382–385. https://doi.org/10.1190/1.1893867

Zelt, C.A., Smith, R.B., 1992. Seismic traveltime inversion for 2-D crustal velocity structure. Geophysical Journal International 108, 16–34. https://doi.org/10.1111/j.1365-246X.1992.tb00836.x

Zhang, J., Wu, J., Li, X., 2013. Compensation for absorption and dispersion in prestack migration: An effective Q approach. GEOPHYSICS 78, S1–S14. https://doi.org/10.1190/geo2012-0128.1

Zhu, T., Harris, J.M., Biondi, B., 2014. *Q* -compensated reverse-time migration. GEOPHYSICS 79, S77–S87. https://doi.org/10.1190/geo2013-0344.1

Highlights

- Reverse time migration method with offshore Wide-Angle seismic.
- Imaging of deep structures as Moho discontinuity and basement of the basin. with reverse time migration method.
- Essential contribution of the refracted wave-field that allow to image the deep structures.
- Effectiveness of the reverse time migration method for wide angle data.
- Essential contribution in the absence of high resolution seismic data, since it is possible to image the deep structures without loosing the imaging of the shallow ones.

Declaration of interests

☐ The authors declare that they have no known competing financial interests or personal relationships that could have appeared to influence the work reported in this paper.

☒ The authors declare the following financial interests/personal relationships which may be considered as potential competing interests:

Susana Goncalves reports financial support was provided by Fundação para a Ciência e Tecnologia (FCT), Portugal. This research was funded by Petrobras (Brazil) and Ifremer (France). The data set collected during the MAGIC and SALSA experiments are protected under a partnership with Petrobras. Any request has to be addressed to Daniel Aslanian (aslanian@ifremer.fr) and Adriano Viana (aviana@petrobras. com.br).